Supplementary Information
to the paper "Achieving High Polarization of Photons Emitted by Unpolarized Electrons in Ultrastrong Laser Fields" by Xian-Zhang Wu, et al.

(Dated: March 28, 2025)

SUPPLEMENTARY NOTE 1: THE APPLIED METHOD FOR SIMULATIONS

We have developed the Monte Carlo code incorporating all polarization effects (including vacuum birefringence and vacuum dichroism) to simulate polarization changes of photons in strong laser field. In the ultraintense laser fields, i.e. the invariant laser field parameter $a_0 \equiv |e|E_0/(m\omega_0) \gg 1$, the formation length of radiation and pair production are much smaller than the laser wavelength and the typical size of the electron (positron) trajectory, making the local constant field approximation (LCFA) valid for simulations[1–3]. Here, E_0 is the laser field amplitude, ω_0 the laser frequency, and e, m the electron charge and mass, respectively. Relativistic units $\hbar = c = 1$ are used throughout. Photon emissions and pair productions are treated quantum mechanically. The photon emission (the pair production) probability is determined by the local electron trajectory, consequently, by the local value of the quantum parameter $\chi_{e,\gamma} \equiv |e|\sqrt{-(F_{\mu\nu}p^{\nu})^2}/m^3$ with the field tensor $F_{\mu\nu}$ and 4-momentum of electron (photon) p^{ν}. We use the quantum probabilities derived with Baier-Katkov QED operator method under LCFA [2]. The photon emission probability is dependent on electron (positron) spin states before and after radiation, and polarization of emitted photon. The pair production probability involves polarization of the parent photon and spin states of the created pair. The energy and polarization of the emitted photons and newly-born particles are determined by the spectral probabilities with random numbers. The moving direction of the emitted photon (newly-born particle) is along that of emitting particle (parent particle) in relativistic regime.

At each time step, the electron (positon) polarization vector $\boldsymbol{S}_i$ jumps to $\boldsymbol{S}_f^R$ after a photon emission. Here, the 3-vector $\boldsymbol{S}_i^R$ ($\boldsymbol{S}_f^R$) denotes the electron spin polarization vector in a mixed state before (after) radiation in its rest frame, corresponding to the electron average polarization state resulting from the scattering process itself [4]. When a photon emission does not take place at the given time step, nevertheless, the electron spin varies to the state of $\boldsymbol{S}_f^{NR}$ according to the no-emission probability, which follows from the one-loop contribution to the electron mass operator [5–7]. Besides, spin precession between emissions is governed by the Thomas-Bargmann-Michel-Telegdi (TBMT) equation [8], where a field dependent anomalous magnetic is included as a result of the one-loop vertex correction [9]. Meanwhile, between quantum events of photon emissions, the electron (positron) dynamics in the laser field is described classically by the Lorentz equation.

The simulation method mentioned above is developed in our previous paper [10–12]. In this work, we enhance the Monte Carlo code for simulating photon polarization dynamics during strong-field QED processes, building upon the algorithm introduced in [13–16]. This enhancement includes the incorporation of vacuum birefringence (VB) and vacuum dichroism (VD), which are manifestations of QED in extreme conditions. In such conditions, the photon dispersion relation is altered by the background field through radiative corrections induced by virtual particles.

A. Algorithm of event generation for photon emission

We use the photon emission probability fomula as follows [17]:

$$\frac{\mathrm{d}^2 W_{rad}}{\mathrm{d}u\mathrm{d}t} = \frac{C_R}{4}\left(F_0 + \boldsymbol{\xi}\cdot\mathbf{F}\right), \tag{S1}$$

where $C_R = \alpha m/\left[\sqrt{3}\pi\gamma_e(1+u)^3\right]$, α is the fine structure constant, γ_e the electron Lorentz factor, $u = \omega_\gamma/\left(\varepsilon_i - \omega_\gamma\right)$, ω_γ the emitted photon energy, ε_i the electron energy before radiation, respectively. The variables introduced in Eq. (S1) read:

$$\begin{aligned}
F_0 &= -(1+u)\mathrm{IntK}_{\frac{1}{3}}(u') + (u^2+2u+2)\mathrm{K}_{\frac{2}{3}}(u') \\
&\quad -u(\mathbf{S}_i\cdot\hat{\mathbf{e}}_2)\mathrm{K}_{\frac{1}{3}}(u') - \mathbf{S}_f\Big\{(1+u)\Big[\mathrm{IntK}_{\frac{1}{3}}(u') - 2\mathrm{K}_{\frac{2}{3}}(u')\Big]\mathbf{S}_i \\
&\quad +u(1+u)\mathrm{K}_{\frac{1}{3}}(u')\hat{\mathbf{e}}_2 + u^2\Big[\mathrm{IntK}_{\frac{1}{3}}(u') \\
&\quad -\mathrm{K}_{\frac{2}{3}}(u')\Big](\mathbf{S}_i\cdot\hat{\mathbf{e}}_v)\hat{\mathbf{e}}_v\Big\}, && \text{(S2)}\\
F_1 &= (\mathbf{S}_i\cdot\hat{\mathbf{e}}_1)u(1+u)\mathrm{K}_{\frac{1}{3}}(u') + (\mathbf{S}_f\cdot\hat{\mathbf{e}}_1)u\mathrm{K}_{\frac{1}{3}}(u') \\
&\quad +(\mathbf{S}_f\times\mathbf{S}_i)\hat{\mathbf{e}}_v\Big(\frac{u^2}{2}+u\Big)\mathrm{K}_{\frac{2}{3}}(u') - \frac{u^2}{2}\Big\{(\mathbf{S}_i\cdot\hat{\mathbf{e}}_1)(\mathbf{S}_f\cdot\hat{\mathbf{e}}_2) \\
&\quad +(\mathbf{S}_f\cdot\hat{\mathbf{e}}_1)(\mathbf{S}_i\cdot\hat{\mathbf{e}}_2)\Big\}\mathrm{IntK}_{\frac{1}{3}}(u'), && \text{(S3)}\\
F_2 &= -(\mathbf{S}_i\cdot\hat{\mathbf{e}}_v)u\mathrm{IntK}_{\frac{1}{3}}(u') - (\mathbf{S}_f\cdot\hat{\mathbf{e}}_v)u(1+u)\mathrm{IntK}_{\frac{1}{3}}(u') \\
&\quad +\Big[(\mathbf{S}_i\cdot\hat{\mathbf{e}}_v) + (\mathbf{S}_f\cdot\hat{\mathbf{e}}_v)\Big](2+u)u\mathrm{K}_{\frac{2}{3}}(u') \\
&\quad -(\mathbf{S}_f\times\mathbf{S}_i)\hat{\mathbf{e}}_1\Big(\frac{u^2}{2}+u\Big)\mathrm{K}_{\frac{1}{3}}(u') - \frac{u^2}{2}\Big[(\mathbf{S}_i\cdot\hat{\mathbf{e}}_v)(\mathbf{S}_f\cdot\hat{\mathbf{e}}_2) \\
&\quad +(\mathbf{S}_f\cdot\hat{\mathbf{e}}_v)(\mathbf{S}_i\cdot\hat{\mathbf{e}}_2)\Big]\mathrm{K}_{\frac{1}{3}}(u'), && \text{(S4)}\\
F_3 &= (1+u)\mathrm{K}_{\frac{2}{3}}(u') - u(1+u)(\mathbf{S}_i\cdot\hat{\mathbf{e}}_2)\mathrm{K}_{\frac{1}{3}}(u') + (\mathbf{S}_i\cdot\mathbf{S}_f) \\
&\quad \Big(\frac{u^2}{2}+u+1\Big)\mathrm{K}_{\frac{2}{3}}(u') - u(\mathbf{S}_f\cdot\hat{\mathbf{e}}_2)\mathrm{K}_{\frac{1}{3}}(u') \\
&\quad -\frac{u^2}{2}\Big\{(\mathbf{S}_i\cdot\hat{\mathbf{e}}_v)(\mathbf{S}_f\cdot\hat{\mathbf{e}}_v)\mathrm{K}_{\frac{2}{3}}(u') + \Big[(\mathbf{S}_i\cdot\hat{\mathbf{e}}_1)(\mathbf{S}_f\cdot\hat{\mathbf{e}}_1) \\
&\quad -(\mathbf{S}_i\cdot\hat{\mathbf{e}}_2)(\mathbf{S}_f\cdot\hat{\mathbf{e}}_2)\Big]\mathrm{IntK}_{\frac{1}{3}}(u')\Big\}, && \text{(S5)}
\end{aligned}$$

where $u' = 2u/3\chi_e$, $\mathrm{IntK}_{\frac{1}{3}}(u') \equiv \int_{u'}^{\infty}\mathrm{d}z\mathrm{K}_{\frac{1}{3}}(z)$, K_n is the n-order modified Bessel function of the second kind, $\hat{\mathbf{e}}_1$ the unit vector along the direction of the transverse component of electron acceleration, $\hat{\mathbf{e}}_2 = \hat{\mathbf{e}}_v\times\hat{\mathbf{e}}_1$ with $\hat{\mathbf{e}}_v$ the unit vector along the electron velocity, $\mathbf{S}_i$ and $\mathbf{S}_f$ are the electron spin-polarization vectors before and after radiation, respectively, $|\mathbf{S}_{i,f}| \leq 1$.

In a time step Δt, the probability for a electron to emit a photon with energy $\omega_\gamma = \delta\varepsilon_i$ ($0 < \delta < 1$) is calculated with Eq.(S1), i.e. $W_{rad}(\delta) = \sum_{S_i,S_f,\xi} \frac{\mathrm{d}W_{rad}}{\mathrm{d}u\mathrm{d}t}\frac{\mathrm{d}u}{\mathrm{d}\delta}\Delta t$, where $\delta = r_1^3$, with r_1 a random number in [0,1]. Another random number $r_2 \in [0,1]$ is used to determine if a photon is emitted: if $3r_1^2 W_{rad}(r_1) < r_2$, reject emitting a photon; otherwise, emit a photon with energy $\omega_\gamma = \delta\varepsilon_i$. Given the smallness of the emission angle $1/\gamma_e$ for an ultrarelativistic electron, the emitted photon is assumed to move along the electron velocity. Note that an approximation to the leading order of $1/\gamma_e$ is used throughout the paper. More detailed informations on this method and its accuracy have been shown in Ref.[15].

For the given emitted photon energy, the electron final spin is determined by Eq.(S1) with photon polarization summed over, as:

$$\frac{\mathrm{d}^2\overline{W}_{rad}}{\mathrm{d}u\mathrm{d}t} = \frac{C_R}{2}F_0, \tag{S6}$$

$$= F_{00} + \mathbf{S}_f\mathbf{F}_{01}, \tag{S7}$$

where,

$$F_{00} = -(1+u)\mathrm{IntK}_{\frac{1}{3}}(u') + (u^2+2u+2)\mathrm{K}_{\frac{2}{3}}(u') - \mathbf{S}_i\cdot\hat{\mathbf{e}}_2 u\mathrm{K}_{\frac{1}{3}}(u'), \tag{S8}$$

$$\mathbf{F}_{01} = -(1+u)\left[\mathrm{IntK}_{\frac{1}{3}}(u') - 2\mathrm{K}_{\frac{2}{3}}(u')\right]\mathbf{S}_i - u(1+u)\mathrm{K}_{\frac{1}{3}}(u')\hat{\mathbf{e}}_2 - u^2\left[\mathrm{IntK}_{\frac{1}{3}}(u') - \mathrm{K}_{\frac{2}{3}}(u')\right](\mathbf{S}_i\cdot\hat{\mathbf{e}}_v)\hat{\mathbf{e}}_v, \tag{S9}$$

After photon emission, the electron spin jumps to $\boldsymbol{S}_f^R$ determined as:

$$\mathbf{S}_f^R = \frac{\mathbf{F}_{01}}{F_{00}}. \tag{S10}$$

If a photon emission event is rejected, the electron spin is also changed according to the no-emission spin variation:

$$\frac{\mathrm{d}^2\overline{W}_{no-rad}}{\mathrm{d}u\mathrm{d}t} = F_{00}^{\mathrm{no}} + \mathbf{S}_f^{NR}\mathbf{F}_{01}^{\mathrm{no}} \tag{S11}$$

$$\mathbf{S}_f^{NR} = \frac{\mathbf{F}_{01}^{\mathrm{no}}}{F_{01}^{\mathrm{no}}}. \tag{S12}$$

where,

$$F_{00}^{\mathrm{no}} = 1 - \int C_R\left[-(1+u)\mathrm{IntK}_{\frac{1}{3}}(u') + (u^2+2u+2)\mathrm{K}_{\frac{2}{3}}(u') - \mathbf{S}_i\cdot\hat{\mathbf{e}}_2 u\mathrm{K}_{\frac{1}{3}}(u')\right]\mathrm{d}u\Delta t, \tag{S13}$$

$$\mathbf{F}_{01}^{\mathrm{no}} = \mathbf{S}_i\left\{1 - \int C_R\left[-(1+u)\mathrm{IntK}_{\frac{1}{3}}(u') + (u^2+2u+2)\mathrm{K}_{\frac{2}{3}}(u')\right]\mathrm{d}u\Delta t\right\} + \hat{\mathbf{e}}_2\int C_R u\mathrm{K}_{\frac{1}{3}}(u')\mathrm{d}u\Delta t. \tag{S14}$$

After photon emission, the Stokes parameter of $\boldsymbol{\xi} = (\xi_1, \xi_2, \xi_3)$ for a emitted photon with respect to the axes of $\hat{\mathbf{e}}_1, \hat{\mathbf{e}}_2$ is determined to be:

$$\boldsymbol{\xi} = \frac{\mathbf{F}}{F_0}, \tag{S15}$$

where $\mathbf{F} = (F_1, F_2, F_3)$.

B. Algorithm of event generation for pair production

Similar with the algorithm for photon emission, we firstly use the total the pair production probability with the pair spin states summed up to determine whether a pair is created or not, then use the specific probability to determine the pair spin states. The pair production probability depending on the initial photon polarization is [2]

$$\begin{aligned}\frac{\mathrm{d}^2\overline{W}_{pair}}{\mathrm{d}\varepsilon_+\mathrm{d}t} &= C_P\{|\mathbf{e}\hat{\mathbf{e}}_1|^2[(\frac{\omega_\gamma^2}{\varepsilon_+\varepsilon_-} - 3)\mathrm{K}_{\frac{2}{3}}(\rho) + \mathrm{IntK}_{\frac{1}{3}}(\rho)] + |\mathbf{e}\hat{\mathbf{e}}_2|^2[(\frac{\omega_\gamma^2}{\varepsilon_+\varepsilon_-} - 1)\mathrm{K}_{\frac{2}{3}}(\rho) + \mathrm{IntK}_{\frac{1}{3}}(\rho)]\} \\ &= C_P\{|\boldsymbol{\xi}|[(\frac{\omega_\gamma^2}{\varepsilon_+\varepsilon_-} - 2)\mathrm{K}_{\frac{2}{3}}(\rho) + \mathrm{IntK}_{\frac{1}{3}}(\rho)] - \xi_3\mathrm{IntK}_{\frac{2}{3}}(\rho)\},\end{aligned} \tag{S16}$$

where $C_p = \alpha m^2/(\sqrt{3}\pi\omega_\gamma^2)$, $\mathbf{e}$ indicates the photon polarization state[18], ω_γ, ε_+ and ε_- the energies of the photon, positron and electron, respectively, with $\omega_\gamma = \varepsilon_+ + \varepsilon_-$, and $\rho = 2\omega_\gamma^2/(3\chi_\gamma\varepsilon_+\varepsilon_+)$. Then the pair production probability is

$$\frac{\mathrm{d}^2\overline{W}_{pair}}{\mathrm{d}\varepsilon_+\mathrm{d}t} = C_P\left\{\left[(\frac{\omega_\gamma^2}{\varepsilon_+\varepsilon_-} - 2)\mathrm{K}_{\frac{2}{3}}(\rho) + \mathrm{IntK}_{\frac{1}{3}}(\rho)\right] - \xi_3\mathrm{IntK}_{\frac{2}{3}}(\rho)\right\}, \tag{S17}$$

Removing the last item from Eq.(S17), the widely employed pair production probability [19] neglecting the photon poalrization is obtained.

The spin state of a created positron is determined by the probability involving photon-polarization and positron spin,

$$\frac{\mathrm{d}^2W_{pair}}{\mathrm{d}\varepsilon_+\mathrm{d}t} = \frac{C_P}{2}\left(F_0^P + \boldsymbol{\xi}\cdot\mathbf{F}^P\right), \tag{S18}$$

where, $F_0^P = [\omega_\gamma^2/(\varepsilon_+\varepsilon_-) - 2]\mathrm{K}_{\frac{2}{3}}(\rho) + \mathrm{IntK}_{\frac{1}{3}}(\rho) + \omega_\gamma/\varepsilon_+(\mathbf{S}_+\cdot\hat{\mathbf{e}}_2)\mathrm{K}_{\frac{1}{3}}(\rho)$, and $\mathbf{F}^P = (F_1^P, F_2^P, F_3^P)$, with

$$F_1^P = \frac{\omega_\gamma}{\varepsilon_-}(\mathbf{S}_+\cdot\hat{\mathbf{e}}_1)\mathrm{K}_{\frac{1}{3}}(\rho), \tag{S19}$$

$$F_2^P = [\frac{\omega_\gamma}{\varepsilon_+}\mathrm{IntK}_{\frac{1}{3}}(\rho) + \frac{{\varepsilon_+}^2 - {\varepsilon_-}^2}{\varepsilon_+\varepsilon_-}\mathrm{K}_{\frac{2}{3}}(\rho)](\mathbf{S}_+\cdot\hat{\mathbf{e}}_v), \tag{S20}$$

$$F_3^P = -\mathrm{K}_{\frac{2}{3}}(\rho) - \frac{\omega_\gamma}{\varepsilon_-}(\mathbf{S}_+\cdot\hat{\mathbf{e}}_2)\mathrm{K}_{\frac{1}{3}}(\rho), \tag{S21}$$

Eq.(S18) can be rewritten in the form similar to Eq.(S1) as:

$$\frac{\mathrm{d}^2 W_{pair}}{\mathrm{d}\varepsilon_+ \mathrm{d}t} = \frac{C_P}{2}\left(\tilde{F}_0^P + \boldsymbol{S}_+ \cdot \tilde{\mathbf{F}}\right) \tag{S22}$$

where, $\tilde{F}_0^P = [\omega_\gamma^2/(\varepsilon_+\varepsilon_-) - 2]\mathrm{K}_{\frac{2}{3}}(\rho) + \mathrm{IntK}_{\frac{1}{3}}(\rho) - \xi_3\mathrm{K}_{\frac{2}{3}}(\rho)$, and $\tilde{\mathbf{F}} = \xi_1\omega_\gamma/\varepsilon_-\mathrm{K}_{\frac{1}{3}}(\rho)\hat{\mathbf{e}}_1 + (\omega_\gamma/\varepsilon_+ - \xi_3\omega_\gamma/\varepsilon_-)\mathrm{K}_{\frac{1}{3}}(\rho)\hat{\mathbf{e}}_2 + \xi_2[\omega_\gamma/\varepsilon_+\mathrm{IntK}_{\frac{1}{3}}(\rho) + ({\varepsilon_+}^2 - {\varepsilon_-}^2)/(\varepsilon_+\varepsilon_-)\mathrm{K}_{\frac{2}{3}}(\rho)]\hat{\mathbf{e}}_v$. The spin state of $\boldsymbol{S}_+$ is determined to be:

$$\boldsymbol{S}_+ = \frac{\tilde{\mathbf{F}}}{\tilde{F}_0^P}. \tag{S23}$$

The spin states of the electron from a pair is also determined by Eqs.(S18)-(S21), by changing ε_+, ε_-, $\mathbf{S}_+$ and $\hat{\mathbf{e}}_{1,2}$ to ε_-, ε_+, $\mathbf{S}_-$ and $-\hat{\mathbf{e}}_{1,2}$, respectively.

C. Particle dynamics in the external laser field between photon emissions or after pair production.

Between quantum events, the electron dynamics in the ultraintense laser field are described by Lorentz equations, $\mathrm{d}\mathbf{p}/\mathrm{d}t = e(\mathbf{E} + \beta \times \mathbf{B})$. The spin precession is governed by the Thomas-Bargmann-Michel-Telegdi equation [8]:

$$\begin{aligned}\frac{\mathrm{d}\mathbf{S}}{\mathrm{d}t} &= \frac{e}{m}\mathbf{S} \times \left[-\left(\frac{g}{2} - 1\right)\frac{\gamma}{\gamma+1}(\boldsymbol{v}\cdot\mathbf{B})\boldsymbol{v}\right. \\ &\left. + \left(\frac{g}{2} - 1 + \frac{1}{\gamma}\right)\mathbf{B} - \left(\frac{g}{2} - \frac{\gamma}{\gamma+1}\right)\boldsymbol{v}\times\mathbf{E}\right],\end{aligned} \tag{S24}$$

where $\mathbf{E}$ and $\mathbf{B}$ are the laser electric and magnetic fields, respectively, g is the electron gyromagnetic factor: $g(\chi_e) = 2 + 2\mu(\chi_e)$, $\mu(\chi_e) = \frac{\alpha}{\pi\chi_e}\int_0^\infty \frac{y}{(1+y)^3}\mathbf{L}_{\frac{1}{3}}\left(\frac{2y}{3\chi_e}\right)\mathrm{d}y$, with $\mathbf{L}_{\frac{1}{3}}(z) = \int_0^\infty \sin\left[\frac{3z}{2}\left(x + \frac{x^3}{3}\right)\right]\mathrm{d}x$. As $\chi_e \ll 1$, $g \approx 2.00232$.

D. Vacuum Polarization Effect in Ultrastrong Laser Field

When a strong laser field is applied to the vacuum, these virtual particle-antiparticle pairs can become polarized, aligning themselves in a way similar to the molecules in a birefringent material. Birefringence in materials causes them to have different refractive indices for light polarized in different directions, and similarly, vacuum birefringence (VB) would cause the vacuum to have different properties for light with different polarizations. Dichroism, on the other hand, refers to the differential absorption of light depending on its polarization. In the context of vacuum dichroism (VD) induced by a strong laser field, this would mean that the vacuum could absorb or attenuate photons differently based on their polarization. In QED terms, these processes result from interference between the tree-level and one-loop propagator diagrams. We describe this effect quantitatively using the following formulas, derived from the no-pair-production probability (see Sec. II for the derivation of the no-pair-production probability).

Following the description of Ref.[20] the VB is treated as:

$$\begin{pmatrix} \xi_{f,1} \\ \xi_{f,2} \end{pmatrix} = \begin{pmatrix} \cos\delta\phi & -\sin\delta\phi \\ \sin\delta\phi & \cos\delta\phi \end{pmatrix}\begin{pmatrix} \xi_{i,1} \\ \xi_{i,2} \end{pmatrix}. \tag{S25}$$

where, $\delta\phi = \phi_1 - \phi_2$ calculated via the following formulas:

$$\phi_i = -\frac{1}{2kq}\,\mathrm{Re}\left[p_i(\chi_\gamma)\right]\Delta\eta. \tag{S26}$$

with

$$\begin{bmatrix} p_1(\eta,\chi_\gamma) \\ p_2(\eta,\chi_\gamma) \end{bmatrix} = \frac{\alpha m^2}{3\pi}\int_{-1}^{+1} dv \begin{bmatrix} (w-1) \\ (w+2) \end{bmatrix}\frac{f'(w')}{w'}, \tag{S27}$$

$w = 4/\left(1 - v^2\right)$, $w' = [w/\chi_\gamma]^{2/3}$, $f(w') = \pi[\mathrm{Gi}(w') + i\,\mathrm{Ai}(w')]$, with $\eta = \omega_0 t - k_0 z$ being the laser phase.

The VD is achieved through a no-pair-production-evolution originating from the intrinsic physical process in which photons with specific polarization states are absorbed with differing probabilities. This polarization-dependent absorption results in the evolution of the polarization of the surviving photons, which can be described by the no-pair-production probability of [7, 16, 21, 22]:

$$W_{\mathrm{noP}} = F_0^L + \boldsymbol{\xi}_f \cdot \mathbf{F}^L, \tag{S28}$$

with

$$\begin{aligned} F_0^L &= \frac{1}{2}\left\{1 - \int_0^1 dx C_p \left[\left(\frac{x}{1-x} + \frac{1-x}{x}\right)\mathrm{K}_{\frac{2}{3}}(\rho)\right.\right. \\ &\left.\left. + \mathrm{IntK}_{\frac{1}{3}}(\rho) - \xi_3\mathrm{K}_{\frac{2}{3}}(\rho)\right]\Delta t\right\}, \end{aligned} \tag{S29}$$

$$\begin{aligned} \mathbf{F}^L &= \frac{1}{2}\left\{\boldsymbol{\xi}_i\left[1 - \int_0^1 dx C_p \left(\mathrm{IntK}_{\frac{1}{3}}(\rho) + \left(\frac{x}{1-x}\right.\right.\right.\right. \\ &\left.\left.\left.\left. + \frac{1-x}{x}\right)\mathrm{K}_{\frac{2}{3}}(\rho)\right)\Delta t\right] + \int_0^1 dx C_p \hat{\mathbf{e}}'_3 \mathrm{K}_{\frac{2}{3}}(\rho)\Delta t\right\} \end{aligned} \tag{S30}$$

where $\hat{\mathbf{e}}'_3 = (0, 0, 1)$.

Thus, we can get the no-pair-production-evolution of [21, 22]:

$$\boldsymbol{\xi}_f = \frac{\mathbf{F}^L}{F_0^L}, \tag{S31}$$

namely,

$$\boldsymbol{\xi}_f = \frac{\boldsymbol{\xi}_i\left\{1-\int_0^1 dxC_p\left[\mathrm{IntK}_{\frac{1}{3}}(\rho)+(\frac{x}{1-x}+\frac{1-x}{x})\mathrm{K}_{\frac{2}{3}}(\rho)\right]\Delta t\right\}+\int_0^1 dxC_p\hat{\mathbf{e}}_3'\mathrm{K}_{\frac{2}{3}}(\rho)\Delta t}{1-\int_0^1 dxC_p\left[(\frac{x}{1-x}+\frac{1-x}{x})\mathrm{K}_{\frac{2}{3}}(\rho)+\mathrm{IntK}_{\frac{1}{3}}(\rho)-\xi_3\mathrm{K}_{\frac{2}{3}}(\rho)\right]\Delta t}$$
$$\approx \boldsymbol{\xi}_i\left\{1+\int_0^1 dxC_p\left[(\frac{x}{1-x}+\frac{1-x}{x})\mathrm{K}_{\frac{2}{3}}(\rho)+\mathrm{IntK}_{\frac{1}{3}}(\rho)-\xi_3\mathrm{K}_{\frac{2}{3}}(\rho)\right]\Delta t\right\} \tag{S32}$$
$$+\left\{\int_0^1 dxC_p\hat{\mathbf{e}}_3'\mathrm{K}_{\frac{2}{3}}(\rho)-\boldsymbol{\xi}_i\int_0^1 dxC_p\left[\mathrm{IntK}_{\frac{1}{3}}(\rho)+(\frac{x}{1-x}+\frac{1-x}{x})\mathrm{K}_{\frac{2}{3}}(\rho)\right]\right\}\Delta t$$
$$= \boldsymbol{\xi}_i+\int_0^1 dxC_p\mathrm{K}_{\frac{2}{3}}(\rho)[\hat{\mathbf{e}}_3'-\boldsymbol{\xi}_i\xi_3]\Delta t.$$

The accuracy of our approach has been confirmed by recalculating the results from Ref. [20], as shown in Figs. S1-S3, a special case where the authors use the polarization operator method in a nonperturbative approach to calculate photon polarization for a whole beam, incorporating the effects of a strong external laser field on the photon propagator and accounting for vacuum birefringence and dichroism.

The no-pair-production evolution method in our work is analogous to the no-emission-spin variation observed in electrons, as both depend on polarization-dependent probabilities. These effects result from interference between the tree-level and one-loop diagrams in QED, and both can be described using no-radiation (or no-pair-production) probabilities.

SUPPLEMENTARY NOTE 2: QED TREATMENT FOR THE NO-PAIR-PRODUCTION PROBABILITY

The QED loop contribution was calculated using the LCFA method, following [7]. The leading-order loop contribution is

$$\mathbb{P}^0 = \frac{1}{2}(1+\boldsymbol{\xi}^i\cdot\boldsymbol{\xi}^f) \tag{S33}$$

Here, $\boldsymbol{\xi}^i$ and $\boldsymbol{\xi}^f$ represent the initial and final states of the photon's Stokes vector, respectively.The $O(\alpha)$-order loop contribution with the interference diagram is

$$\mathbb{P}^{\mathrm{L}} = \langle\mathbb{P}^{\mathrm{L}}\rangle+\mathbf{P}_0^{\mathrm{L}}\cdot\mathbf{n}_0+\mathbf{P}_1^{\mathrm{L}}\cdot\mathbf{n}_1+\mathbf{n}_1\cdot\mathbf{P}_{10}^{\mathrm{L}}\cdot\mathbf{n}_0, \tag{S34}$$

where $\mathbf{n}_0=\boldsymbol{\xi}^i, \mathbf{n}_1=\boldsymbol{\xi}^f$. Under the linearly polarized laser field, the components of Eq.(S34) are as follows:

$$\{\langle\mathbb{P}^{\mathrm{L}}\rangle,\mathbf{P}_0^{\mathrm{L}},\ldots\} = \frac{\alpha}{2}\int\frac{\mathrm{d}\sigma}{b_0}\int_0^1\mathrm{d}s\{\langle\hat{\mathbb{R}}^{\mathrm{L}}\rangle,\hat{\mathbf{R}}_0^{\mathrm{L}},\ldots\}, \tag{S35}$$

$$\langle\hat{\mathbb{R}}^{\mathrm{L}}\rangle = -\mathrm{Ai}_1(\xi)+\kappa\frac{\mathrm{Ai}'(\xi)}{\xi}, \tag{S36}$$

$$\hat{\mathbf{R}}_0^{\mathrm{L}} = \hat{\mathbf{R}}_1^{\mathrm{L}} = -\frac{\mathrm{Ai}'(\xi)}{\xi}\boldsymbol{\epsilon}_{\mathrm{E}}, \tag{S37}$$

$$\hat{\mathbf{R}}_{10,ij}^{\mathrm{L}} = \langle\hat{\mathbb{R}}^{\mathrm{L}}\rangle\mathbf{1}+\frac{\mathrm{Gi}'(\xi)}{\xi}\varepsilon_{3ij}, \tag{S38}$$

where $s=\varepsilon/\omega$, ε, ε_+ and ω are the energy of produced electrons, positrons and seed photons, respectively; $\xi=(r/\chi_\gamma)^{2/3}$, $\chi_\gamma\equiv|e|\sqrt{-(F_{\mu\nu}k^\nu)^2}/m^3$ is quantum parameter; $b_0=kq$ is the dimensionless longitudinal momentum of the original particle that entered the laser, $\mathrm{Ai}_1(\xi)=\int_\xi^\infty \mathrm{d}t\mathrm{Ai}(t)$, $\kappa=\frac{s}{1-s}+\frac{1-s}{s}$, $r=\frac{1}{s}+\frac{1}{1-s}$, $\boldsymbol{\epsilon}_{\mathrm{E}}=\{0,0,1\}$; ε_{3ij} is the Levi-Civita tensor with $\varepsilon_{123}=1$; $\mathrm{Ai}(x)$ and $\mathrm{Gi}(x)$ are the Airy function and the Scorer Gi function, respectively.

Here,

$$\mathrm{Ai}(x) = \frac{1}{\pi}\sqrt{\frac{x}{3}}K_{1/3}\left(\frac{2}{3}x^{3/2}\right), \tag{S39}$$

$$\mathrm{Ai}'(x) = -\frac{x^{1/2}}{\pi\sqrt{3}}K_{2/3}\left(\frac{2}{3}x^{3/2}\right), \tag{S40}$$

K_i is The modified Bessel function of the third kind of order i. Then

$$\mathrm{Ai}_1(\xi) = \frac{1}{\pi\sqrt{3}}\int_\rho^\infty dx\mathrm{K}_{\frac{1}{3}}(x) = \frac{1}{\pi\sqrt{3}}\mathrm{IntK}_{\frac{1}{3}}(\rho), \tag{S41}$$

$$\frac{\mathrm{Ai}'(\xi)}{\xi} = -\frac{1}{\pi\sqrt{3}}\mathrm{K}_{\frac{2}{3}}(\rho), \tag{S42}$$

where $\rho=\frac{2}{3\chi_\gamma}\frac{\omega^2}{\varepsilon_+\varepsilon}$.

Then, we substitute Eq.(S36) to Eq.(S38) into Eq.(S35) and assume that the time step Δt is extremely short. The sum of these contributions is

$$\begin{aligned}\mathbb{P} =&\mathbb{P}^0 + \mathbb{P}^{\mathrm{L}}\\ =&\frac{1}{2}\left(1-\int_0^1 dsC_p\left[\mathrm{IntK}_{\frac13}(\rho)+\frac{s^2+(1-s)^2}{s(1-s)}\mathrm{K}_{\frac23}(\rho) \;-\mathrm{K}_{\frac23}(\rho)\hat{\mathbf{e}}_3\cdot\boldsymbol{\xi}^i\right]\Delta t\right)+\\ &\frac12\boldsymbol{\xi}^f\left[\left(1-\int_0^1 dsC_p\left[\mathrm{IntK}_{\frac13}(\rho)+\frac{s^2+(1-s)^2}{s(1-s)}\mathrm{K}_{\frac23}(\rho)\right]\Delta t\right)\boldsymbol{\xi}^i+\int_0^1 dsC_p\mathrm{K}_{\frac23}(\rho)\hat{\mathbf{e}}_3\Delta t\right]+\frac{\alpha m^2}{2\omega}\Delta t\int_0^1 ds\frac{\mathrm{Gi}'(u)}{u}\boldsymbol{\xi}^i\varepsilon_{3ij}\boldsymbol{\xi}^f\end{aligned}\tag{S43}$$

which can be writen as,

$$\mathbb{P} = P^L_{VD} + P^L_{VB}\tag{S44}$$

with

$$\begin{aligned}P^L_{VD} =&\frac{1}{2}\left(1-\int_0^1 dsC_p\left[\mathrm{IntK}_{\frac13}(\rho)+\frac{s^2+(1-s)^2}{s(1-s)}\mathrm{K}_{\frac23}(\rho) \;-\mathrm{K}_{\frac23}(\rho)\hat{\mathbf{e}}_3\cdot\boldsymbol{\xi}^i\right]\Delta t\right)+\\ &\frac12\boldsymbol{\xi}^f\left[\left(1-\int_0^1 dsC_p\left[\mathrm{IntK}_{\frac13}(\rho)+\frac{s^2+(1-s)^2}{s(1-s)}\mathrm{K}_{\frac23}(\rho)\right]\Delta t\right)\boldsymbol{\xi}^i+\int_0^1 dsC_p\mathrm{K}_{\frac23}(\rho)\hat{\mathbf{e}}_3\Delta t\right]\end{aligned}\tag{S45}$$

$$P^L_{VB} =\frac{\alpha m^2}{2\omega}\Delta t\int_0^1 ds\frac{\mathrm{Gi}'(u)}{u}\boldsymbol{\xi}^i\varepsilon_{3ij}\boldsymbol{\xi}^f \quad =\frac{\alpha m^2}{2\omega}\Delta t\int_0^1 ds\frac{\mathrm{Gi}'(u)}{u}(\xi_2^i\xi_1^f-\xi_1^i\xi_2^f),\tag{S46}$$

where $C_p = \frac{\alpha m^2}{\sqrt{3}\pi\omega}$; $u = \frac{1}{[s(1-s)\chi_\gamma]^{2/3}}$; $\hat{\mathbf{e}}_3 = \{0,0,1\}$and $\mathrm{Gi}'(x)$ is the Scorer prime function.

The first term in Eq.(S44), P^L_{VD}, same as Eq. (S28), originates from the imaginary part of the polarization operator, corresponding to the no-pair-production probability used for describing "vacuum dichroism". The second term, P^L_{VB}, is associated with the real part of the polarization operator and gives rise to "vacuum birefringence".

SUPPLEMENTARY NOTE 3: DERIVATION OF THE EQ. (1) IN THE MAIN TEXT

The Eq. (1) in the main text can be obtained from Eq.(S32):

$$\begin{aligned}\frac{d\xi_3}{dt} &= \lim_{\Delta t\to 0}\frac{\xi_3^f-\xi_3^i}{\Delta t}\\ &= (1-\xi_3^2)\int_0^1 dxC_p\mathrm{K}_{\frac23}(\rho).\end{aligned}\tag{S47}$$

Its accuracy is confirmed by recalculating the result in Ref.[20] as shown in Fig.S2. We have plotted the result of ξ_3 in Ref. [20] with the method of the reference but employing Eq (3) in our manuscript instead. The result is coincident with that in Ref.[20], with a tiny difference as exhibited in Fig. S3.

SUPPLEMENTARY NOTE 4: THEORETICAL EXPLANATION FOR THE POLARIZATION ENHANCEMENT FROM THE PURE STATE PERSPECTIVE

For a group of high-energy photons of $N_i = N_i^+ + N_i^-$, N_i^+ photons have $\xi_3 = +1$ and N_i^- photons have $\xi_3 = -1$. The initial photon polarization is:

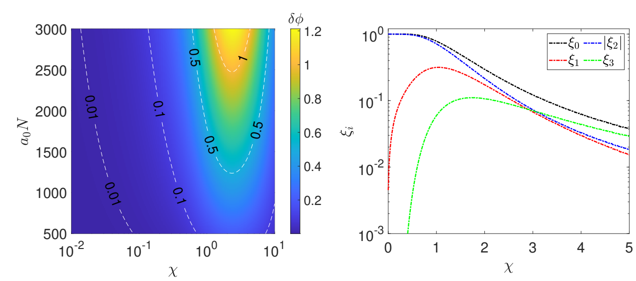

FIG. S1. Reproduction of the previous results, Figs. 4 and 5 of Ref. [20]. (a): Plot of $\delta\phi$ as a function of χ and a_0N for a rectangular pulse profile with N laser periods. (b): Final Stokes parameters for gamma photons propagating through an ELI-NP 10 PW laser pulse with initial $\boldsymbol{\xi} = (1, 0, -1)$.

$$\bar{\xi}_3^i = \frac{N_i^+ - N_i^-}{N_i^+ + N_i^-}.\tag{S48}$$

After a time step of Δt, the pair-production probabilities for $\xi_3 = +1$ photons and $\xi_3 = -1$ photons are:

$$\begin{aligned}W^+_{pair} =& \int_0^1 dxC_p\left[\left(\frac{x}{1-x}+\frac{1-x}{x}\right)\mathrm{K}_{\frac23}(\rho)\right.\\ &\left.+\mathrm{IntK}_{\frac13}(\rho) - \;\mathrm{K}_{\frac23}(\rho)\right]\Delta t,\end{aligned}\tag{S49}$$

and

$$\begin{aligned}W^-_{pair} =& \int_0^1 dxC_p\left[\left(\frac{x}{1-x}+\frac{1-x}{x}\right)\mathrm{K}_{\frac23}(\rho)\right.\\ &\left.+\mathrm{IntK}_{\frac13}(\rho) + \;\mathrm{K}_{\frac23}(\rho)\right]\Delta t.\end{aligned}\tag{S50}$$

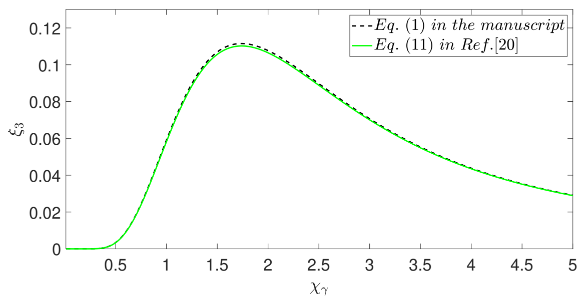

FIG. S2. The results of ξ_3 obtained via Eq. (1) in the manuscript (black-dashed) and via Eq. (11) in Ref. [20] (green-solid).

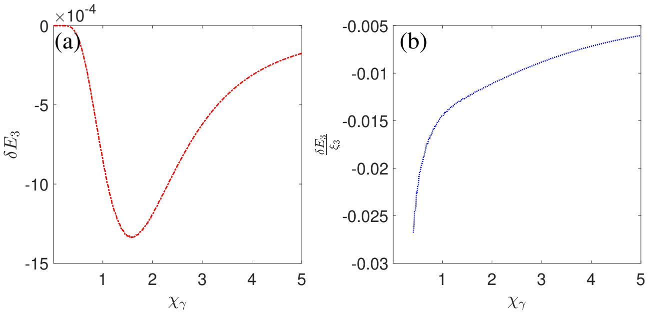

FIG. S3. Error analysis between the results with two methods in Fig.S2. (a): Absolute errors. (b): Relative errors.

The the photon numbers change into:

$$N_f^+ = N_i^+(1 - W_{pair}^+) \tag{S51}$$

$$N_f^- = N_i^-(1 - W_{pair}^-). \tag{S52}$$

Then the photon polarization should be:

$$\overline{\xi}_3^f = \frac{N_f^+ - N_f^-}{N_f^+ + N_f^-}. \tag{S53}$$

We make $C = 1 - \int_0^1 dxC_p \left[\left(\frac{x}{1-x} + \frac{1-x}{x}\right) \mathrm{K}_{\frac{2}{3}}(\rho) + \mathrm{IntK}_{\frac{1}{3}}(\rho)\right] \Delta t$ and $C_1 = \int_0^1 dxC_p\, \mathrm{K}_{\frac{2}{3}}(\rho)\Delta t$ for simplicity, then,

$$\begin{aligned} \overline{\xi}_3^f &= \frac{N_i^+(1 - W_{pair}^+) - N_i^-(1 - W_{pair}^-)}{N_i^+(1 - W_{pair}^+) + N_i^-(1 - W_{pair}^-)} \\ &= \frac{C(N_i^+ - N_i^+) + C_1(N_i^+ + N_i^+)}{C(N_i^+ + N_i^+) + C_1(N_i^+ - N_i^+)} \\ &= \frac{C\overline{\xi}_3^i + C_1}{C + C_1\overline{\xi}_3^i}, \end{aligned} \tag{S54}$$

which is coincident with Eq.(S32).

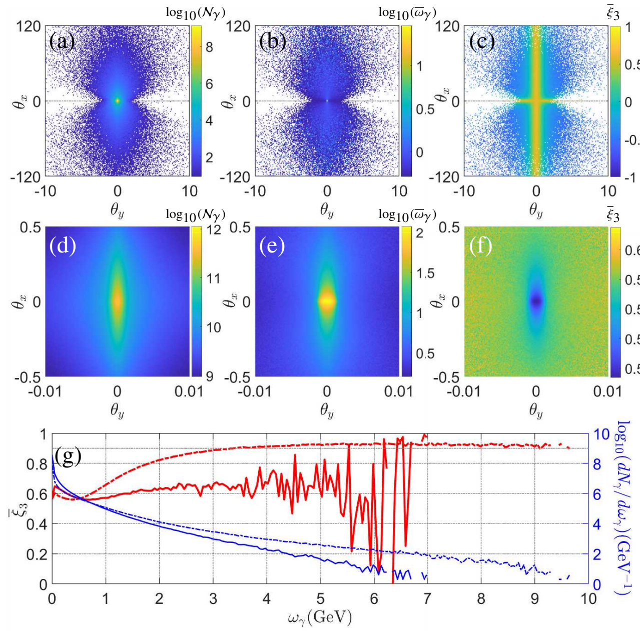

FIG. S4. (a)-(c): Distributions of number density $\log_{10}(\mathcal{N}_\gamma)$, average photon energy $\log_{10}(\bar{\omega}_\gamma)$, and $\overline{\xi}_3$, with respect to scattering angles of $\theta_x \equiv k_x/k_z$ and $\theta_y \equiv k_y/k_z$, for the secondary emitted photons. Here, $\mathcal{N}_\gamma = \mathrm{d}^2N_\gamma/\mathrm{d}\theta_x\, \mathrm{d}\theta_y$. (d)-(f): Distributions of $\log_{10}(\mathcal{N}_\gamma)$, $\log_{10}(\bar{\omega}_\gamma)$, and $\overline{\xi}_3$, for the selected photons with $\theta_x \in [-0.5, 0.5]$ and $\theta_y \in [-0.01, 0.01]$. (g) Polarization of $\overline{\xi}_3$ (red), and $\log_{10}(\mathrm{d}N_\gamma/\mathrm{d}\omega_\gamma)$ (blue) for the selected photons in (d) vs photon energy ω_γ, respectively. The solid and dash-dotted lines indicate the results with secondary photons and primary photons, respectively.

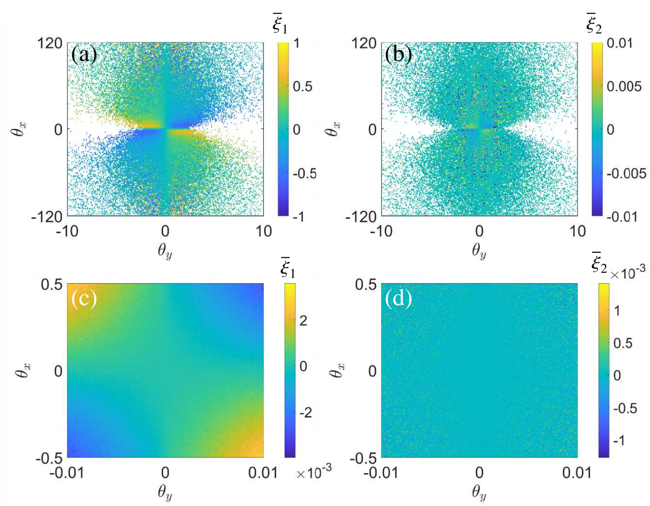

FIG. S5. (a)-(b): Distributions of $\overline{\xi}_1$ and $\overline{\xi}_2$, with respect to scattering angles of θ_x and θ_y, for the whole emitted photons. (c)-(d): Distributions of $\overline{\xi}_1$ and $\overline{\xi}_2$, for the selected photons with $\theta_x \in [-0.5, 0.5]$ and $\theta_y \in [-0.01, 0.01]$.

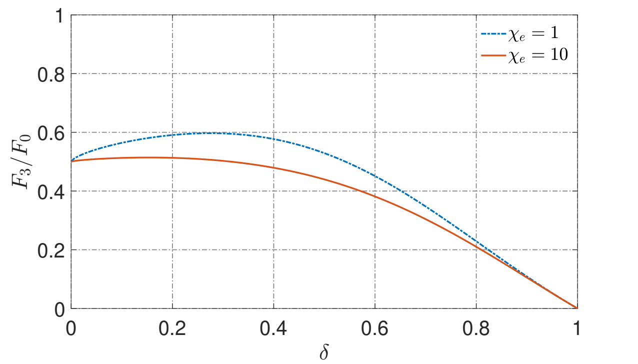

FIG. S6. Photon polarization of $\xi_3 = F_3/F_0$ vs $\delta = \omega_\gamma/\varepsilon_e$ calculated via Eq.(S15). The red solid and blue dash-dotted lines indicate the result with $\chi_e = 10$ and $\chi_e = 1$,respectively.

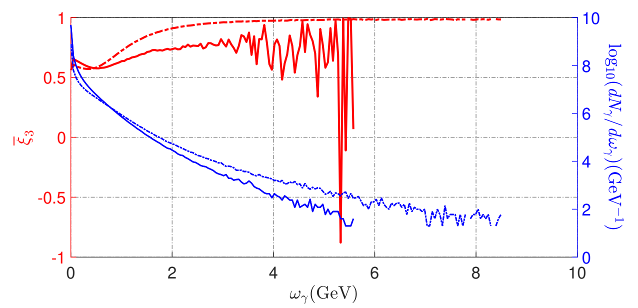

FIG. S7. Polarization of $\bar{\xi}_3$ (red), and $\log_{10}\left(\mathrm{d}N_\gamma/\mathrm{d}\omega_\gamma\right)$ (blue) vs photon energy ω_γ, respectively. The solid and dash-dotted lines indicate the results for the secondary photons and primary photons, respectively.

SUPPLEMENTARY NOTE 5: IMPACT OF THE PHOTONS EMITTED BY THE NEWLY-CREATED PAIRS

The impact of photons emitted by newly-created pairs, referred to as secondary photons compared to the primary photons emitted by the seed electrons, is analyzed in Fig. S4. The secondary photons span a wide range in angular distribution, as shown in Figs. S4(a)-(f), but occupy a relatively narrow range in photon energy distribution, see Fig. S4(g). At low energy levels, the number of secondary photons surpasses that of primary photons, and at medium energy levels, their numbers are comparable. However, at high energy levels, the number of secondary photons is practically zero, indicating that secondary photons can be disregarded in the desired high-energy segment.

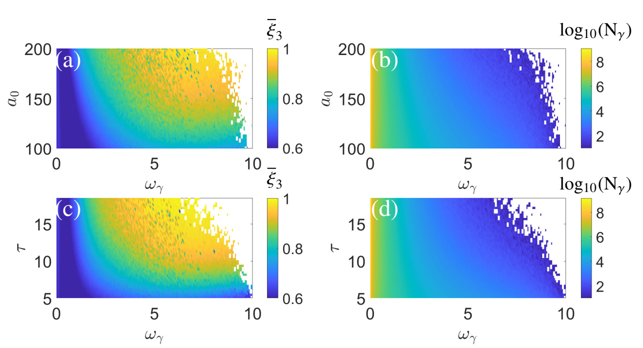

FIG. S8. Distributions of photon polarization and photon number(N_γ) with respect to ω_γ at different a_0 and τ. The other parameters are the same with those in Fig.2 of the paper but with a reduced $N_e = 5 \times 10^5$.

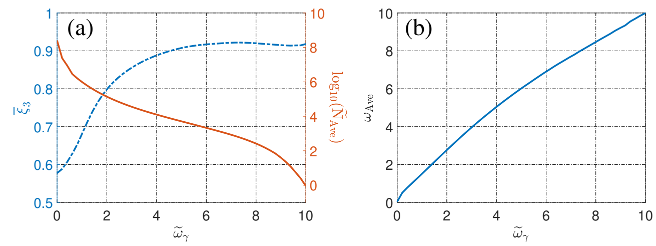

FIG. S9. (a): The average polarization of $\bar{\xi}_3$ and number of $\log_{10}(\mathrm{N}_{\mathrm{Ave}})$ for photons selected within a certain energy range of $\omega_\gamma \in [\tilde{\omega}_\gamma, 10\mathrm{GeV}]$ vs $\tilde{\omega}_\gamma$ in Fig.2 of the paper. (b): The average photon energy for the selected photons.

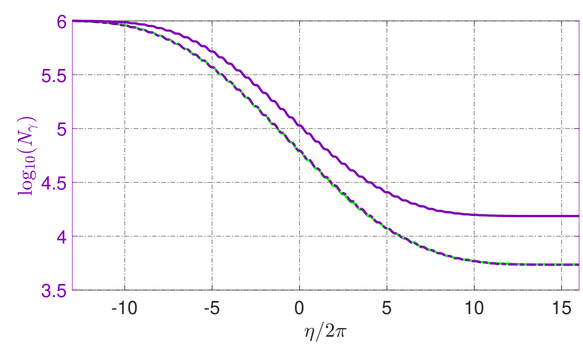

FIG. S10. Evolution of photon number for a γ-ray beam with energies of 10 GeV (dash-dotted) or 5 GeV (solid), numerically calculated using mixed states for ξ. The green curves correspond to numerical results using pure states, where half of the photons have $\xi_3 = +1$ and half have $\xi_3 = -1$.

SUPPLEMENTARY NOTE 6: SIMULATION RESULTS OF PHOTON POLARIZATION COMPONENTS

In Fig. S5, we present the results for $\bar{\xi}_1$ and $\bar{\xi}_2$ based on the same simulation as in Fig. 2 of the paper. Notably, a significant $\bar{\xi}_1$ is observed across a wide range of scattering angles, as depicted in Fig. S5(a). This phenomenon arises from the emission of photons by electrons with $p_\perp \gtrsim p_\parallel$, leading to a substantial difference between $\hat{\mathbf{e}}_1$ and the x-axis. It's important to note that the information regarding ξ_1 and ξ_2 can be simultaneously obtained with ξ_3 when using the mixed state method, which is not achievable when using pure states.

SUPPLEMENTARY NOTE 7: DEPENDENCE OF EMITTED PHOTON POLARIZATION ON PHOTON ENERGY

In Fig.S6, we show the dependence of ξ_3 on δ. As proven by others [17, 23, 24], the ξ_3 decreases with δ, particularly in the larger δ range.

SUPPLEMENTARY NOTE 8: POLARIZATION FOR THE SECONDARY AND PRIMARY PHOTONS IN FIG.4 OF THE PAPER

The polarization of secondary and primary photons in Fig. 4 of the paper is illustrated in Fig. S7, to provide an interpretation for the fluctuation observed in the polarization curve around $\omega_\gamma \approx 5$ GeV. The polarization variability of the secondary photons attributed to statistical uncertainties causes the fluctuation, see Sec. XIV for a more detailed explanation.

SUPPLEMENTARY NOTE 9: POLARIZATION DISTRIBUTIONS WITH RESPECT TO PHOTON ENERGY

Fig.S8 presents distributions of photon polarization and photon number relative to ω_γ under varying a_0 and τ. The photon polarization and number for a certain photon energy vary with the changing of a_0 and τ, and high-energy photons may diminish significantly due to substantial pair production. Consequently, adjusting parameters becomes imperative for a desired γ-ray beam for practical experimental applications.

Another feasible way for better applications of polarized gamma photons is post-energy selection plays. Fig. S9 illustrates the polarization degree, number, and average energy for the selected photons, as discussed.

SUPPLEMENTARY NOTE 10: DISTRIBUTIONS OF PHOTON NUMBER IN FIG.3 (B) OF THE PAPER

The distributions of photon number in Fig.3 (b) of the paper is shown in Fig.S10.

SUPPLEMENTARY NOTE 11: DESCRIPTION OF THE LASER FIELD AND THE ELECTRON BEAM

In this work, we employ tightly-focused laser pulses with a Gaussian temporal profile, which propagate along $+z$ direction as a scattering laser beam. The spatial distribution of the electromagnetic fields takes into account up to ϵ_0^3-order of the nonparaxial solution, where $\epsilon_0 = w_0/z_r$, while w_0 is the laser focal radius, $z_r = k_0 w_0^2/2$ the Rayleigh length with laser wave vector $k_0 = 2\pi/\lambda_0$, and λ_0 the laser wavelength. The expressions of the electromagnetic fields of the linearly-polarized (LP) (along x axis) laser pulse are as follows [25]:

$$
\begin{aligned}
E_x^L &= -iE^L\left[1+\epsilon_0^2\left(f^2\widetilde{x}^2-\frac{f^3\rho^4}{4}\right)\right],\\
E_y^L &= -iE^L\epsilon_0^2 f^2\widetilde{xy},\\
E_z^L &= E^L\left[\epsilon_0 f\widetilde{x}+\epsilon_0^3\widetilde{x}\left(-\frac{f^2}{2}+f^3\rho^2-\frac{f^4\rho^4}{4}\right)\right],\\
B_x^L &= 0,\\
B_y^L &= -iE^L\left[1+\epsilon_0^2\left(\frac{f^2\rho^2}{2}-\frac{f^3\rho^4}{4}\right)\right],\\
B_z^L &= E^L\left[\epsilon_0 f\widetilde{y}+\epsilon_0^3\widetilde{y}\left(\frac{f^2}{2}+\frac{f^3\rho^2}{2}-\frac{f^4\rho^4}{4}\right)\right];\\
\\
E^L &= E_0 F_n f e^{-f\rho^2} e^{i(\eta+\psi_{\rm CEP})} e^{-\frac{t^2}{\tau^2}},
\end{aligned}
\tag{S55}
$$

where τ is the laser pulse duration, E_0 the amplitude of the laser fields with normalization factor $F_n = i$ to keep $\sqrt{(E_x^L)^2+(E_y^L)^2+(E_z^L)^2} = E_0$ at the focus, with scaled coordinates

$$
\widetilde{x}=\frac{x}{w_0},\quad \widetilde{y}=\frac{y}{w_0},\quad \widetilde{z}=\frac{z}{z_r},\quad \rho^2=\widetilde{x}^2+\widetilde{y}^2, \tag{S56}
$$

$f = \frac{i}{\widetilde{z}+i}$, $\eta = \omega_0 t - k_0 z$, and $\psi_{\rm CEP}$ is the carrier-envelope phase.

The electron beam is longitudinally uniformly distributed with a longitudinal length of 3 λ. Its transverse cross-section follows a two-dimensional Gaussian distribution centered at the origin, with $\sigma_x = \sigma_y = 0.3\lambda$. Thus, the electron beam forms a cylinder-like shape.

SUPPLEMENTARY NOTE 12: EXPLANATION FOR THE FLUCTUATIONS IN THE PHOTON ENERGY SPECTRUM

Obvious fluctuations exist in some part of the photon polarization distributions as shown in Fig.4 of the paper and Figs. S4 (g) and S7. The fluctuations are primarily attributed to statistical uncertainties, which can be estimated as $\delta P/P \sim 1/\sqrt{N_\gamma}$. Particularly the fluctuations are more pronounced at the part where the photon number is smaller. For the higher energy range of secondary photons, the photon count decreases significantly (only a few photons per data point), leading to larger statistical fluctuations. When plotting the energy spectrum encompassing both secondary and primary photons, we got obvious fluctuations thereby.

The numerical fluctuations can be reduced by enhancing the initial electron number. As shown in Fig. S11, where we increased the initial electron number by a factor of 10 (i.e., $N_e = 10^7$), the statistical uncertainty was significantly reduced, and the oscillatory pattern became less pronounced compared with Fig. 4(b) and Fig. 2(g).

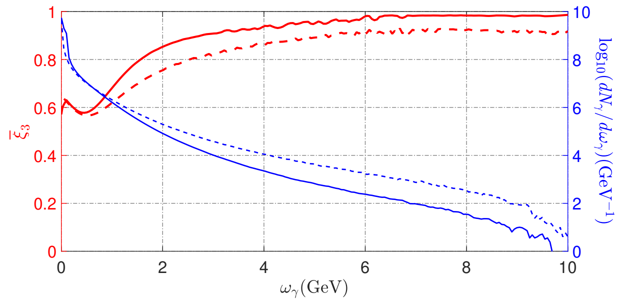

FIG. S11. Photon polarization and number vs ω_γ with $\tau = 15T_0$ and other parameters the same with as in MS Fig.2. The solid line and dashed line represent the results for $\tau = 15T_0$ and $\tau = 10T_0$, respectively.

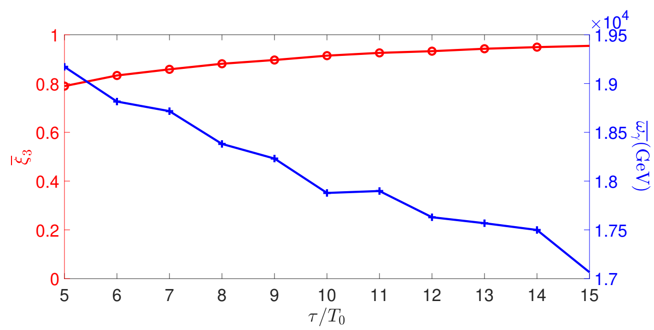

FIG. S12. Under the condition of constant laser energy, the effects of varying the laser pulse duration (intensity) on the polarization and energy of photons. Distributions of average photon polarization and average photon energy vs τ for 0.1% N_e photons selected with highest energies. The other parameters are the same with those in MS Fig.2.

In practical applications, using an electron beam with a charge of approximately 10 pC (typical for laser-driven electron beams), such fluctuations would still exist but with significantly reduced amplitude, as a higher number of interacting particles naturally improves statistical accuracy.

SUPPLEMENTARY NOTE 13: INFLUENCE OF LASER CONDITIONS ON PHOTONS

With a constant laser power P as used in MS Fig. 2, increasing the laser pulse duration τ enhances the photon polarization degree due to a strengthened vacuum dichroism (VD) effect, which scales as $\sim \chi\tau \propto \tau\sqrt{P/\tau} \propto \sqrt{\tau}$. Meanwhile, the energy of emitted photons decreases due to the reduction of a_0, following the relation $\omega_\gamma/\varepsilon_e \sim \chi \propto a_0$ for $\chi < 1$.

To address the concern about impact of laser pointing stability and collision angles, we conducted additional simulations examining the effects of laser pointing instabilities

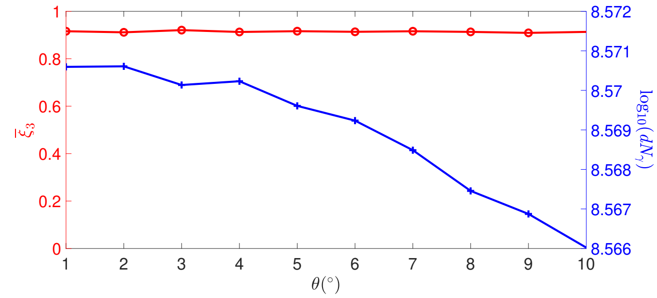

FIG. S13. The impact of the collision angle $(180^\circ - \theta')$ between the electron beam and laser pulse on photon polarization and generation. Distributions of average photon polarization vs θ' for 0.1% N_e photons selected with highest energies(red solid line with a circle) and photon yields vs θ' (blue solid line with +). The other parameters are the same with those in MS Fig.2.

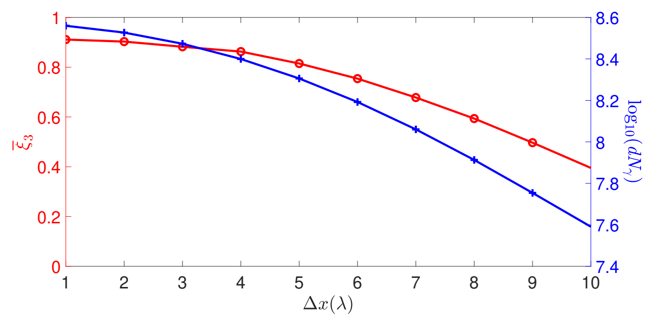

FIG. S14. The impact of the collision position deviation(Δx) between the electron beam and the laser pulse on photon polarization and generation. Distributions of average photon polarization vs Δx for 0.1% N_e photons selected with highest energies(red solid line with a circle) and photon yields vs Δx (blue solid line with +). The other parameters are the same with those in MS Fig.2.

and variations in collision angles as shown in Fig. S13 and Fig. S14. Our results indicate that as the θ' increases, both the photon polarization degree and yield remain stable. In contrast, deviation in the collision position significantly affects photon production rates and polarization, as it determines the efficiency of interaction overlap. Specifically, when the deviation is 10 λ, the photon production rate decreases by an order of magnitude, and the photon polarization drops to approximately 40%.

SUPPLEMENTARY NOTE 14: AVERAGE PHOTON POLARIZATION FOR DIFFERENT SELECTED ENERGY CUT-OFFS

From an application perspective, we present the average photon polarization for different energy cut-offs, as shown in

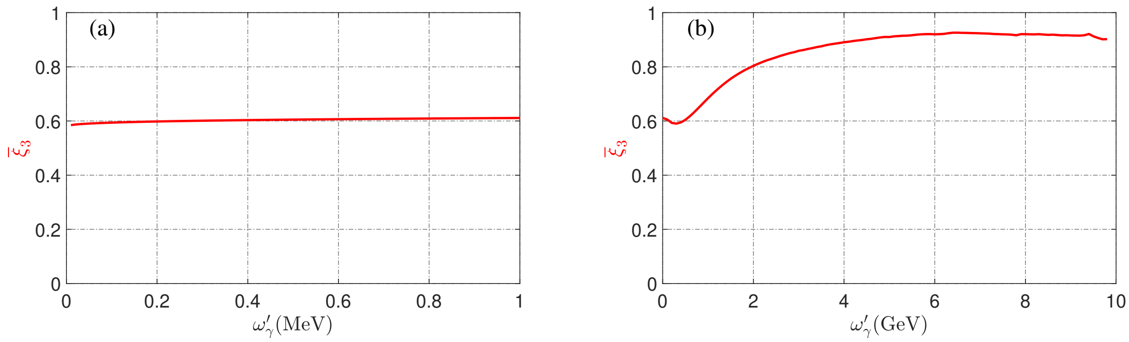

FIG. S15. Average photon polarization with respect to the selected photon energy cutoff (ω'_γ). (a)ω'_γ ranging from 0 to 1 MeV; (b)ω'_γ ranging from 0 to 10 GeV. The average polarization is calculated for photons with energy higher than ω'_γ.

Fig. S15.

SUPPLEMENTARY REFERENCES

[1] V. I. Ritus, J. Sov. Laser Res. **6**, 497 (1985).

[2] V. N. Baier, V. M. Katkov, and V. M. Strakhovenko, *Electromagnetic Processes at High Energies in Oriented Single Crystals* (World Scientific, Singapore, 1998).

[3] M. Kh. Khokonov and I. Z. Bekulova, "Length of formation of processes in a constant external field at high energies," Technical Physics **55**, 728–731 (2010).

[4] V. B. Berestetskii, E. M. Lifshitz, and L. P. Pitaevskii, *Quantum Electrodynamics* (Pergamon, Oxford, 1982).

[5] S. Meuren and A. Di Piazza, "Quantum electron self-interaction in a strong laser field," Phys. Rev. Lett. **107**, 260401 (2011).

[6] A. Ilderton, B. King, and S. Tang, "Loop spin effects in intense background fields," Phys. Rev. D **102**, 076013 (2020).

[7] Greger Torgrimsson, "Loops and polarization in strong-field QED," New J. Phys. **23**, 065001 (2021).

[8] V. Bargmann, Louis Michel, and V. L. Telegdi, "Precession of the polarization of particles moving in a homogeneous electromagnetic field," Phys. Rev. Lett. **2**, 435–436 (1959).

[9] V. N. Baǐer, "Radiative polarization of electrons in storage rings," Sov. Phys. Usp. **14**, 695 (1972).

[10] Yan-Fei Li, Yue-Yue Chen, Wei-Min Wang, and Hua-Si Hu, "Production of highly polarized positron beams via helicity transfer from polarized electrons in a strong laser field," Phys. Rev. Lett. **125**, 044802 (2020).

[11] Yan-Fei Li, Yue-Yue Chen, Karen Z. Hatsagortsyan, and Christoph H. Keitel, "Helicity transfer in strong laser fields via the electron anomalous magnetic moment," Phys. Rev. Lett. **128**, 174801 (2022).

[12] Yan-Fei Li, Yue-Yue Chen, K. Z. Hatsagortsyan, A. Di Piazza, M. Tamburini, and C. H. Keitel, "Strong signature of one-loop self-energy in polarization resolved nonlinear compton scattering," Phys. Rev. D **107**, 116020 (2023).

[13] C.P. Ridgers, J.G. Kirk, R. Duclous, T.G. Blackburn, C.S. Brady, K. Bennett, T.D. Arber, and A.R. Bell, "Modelling gamma-ray photon emission and pair production in high-intensity laser–matter interactions," Journal of Computational Physics **260**, 273 – 285 (2014).

[14] N. V. Elkina, A. M. Fedotov, I. Yu. Kostyukov, M. V. Legkov, N. B. Narozhny, E. N. Nerush, and H. Ruhl, "Qed cascades induced by circularly polarized laser fields," Phys. Rev. ST Accel. Beams **14**, 054401 (2011).

[15] A. Gonoskov, S. Bastrakov, E. Efimenko, A. Ilderton, M. Marklund, I. Meyerov, A. Muraviev, A. Sergeev, I. Surmin, and E. Wallin, "Extended particle-in-cell schemes for physics in ultrastrong laser fields: Review and developments," Phys. Rev. E **92**, 023305 (2015).

[16] User's Manual of CAIN: `https://www-jlc.kek.jp/subg/ir/lib/cain21b.manual/`,.

[17] Yan-Fei Li, Rashid Shaisultanov, Yue-Yue Chen, Feng Wan, Karen Z. Hatsagortsyan, Christoph H. Keitel, and Jian-Xing Li, "Polarized ultrashort brilliant multi-gev γ rays via single-shot laser-electron interaction," Phys. Rev. Lett. **124**, 014801 (2020).

[18] William H. McMaster, "Matrix representation of polarization," Rev. Mod. Phys. **33**, 8–28 (1961).

[19] A. Di Piazza, C. Müller, K. Z. Hatsagortsyan, and C. H. Keitel, "Extremely high-intensity laser interactions with fundamental quantum systems," Rev. Mod. Phys. **84**, 1177–1228 (2012).

[20] Sergey Bragin, Sebastian Meuren, Christoph H. Keitel, and Antonino Di Piazza, "High-energy vacuum birefringence and dichroism in an ultrastrong laser field," Phys. Rev. Lett. **119**, 250403 (2017).

[21] Kai-Hong Zhuang, Yue-Yue Chen, Yan-Fei Li, Karen Z. Hatsagortsyan, and Christoph H. Keitel, "Laser-driven lepton polarization in the quantum radiation-dominated reflection regime," Phys. Rev. D **108**, 033001 (2023).

[22] Ya-Nan Dai, Karen Z. Hatsagortsyan, Christoph H. Keitel, and Yue-Yue Chen, "Fermionic signal of vacuum polarization in strong laser fields," Phys. Rev. D **110**, 012008 (2024).

[23] Suo Tang, Yu Xin, Meng Wen, Mamat Ali Bake, and Baisong Xie, "Fully polarized Compton scattering in plane waves and its polarization transfer," Matter and Radiation at Extremes **9**, 037204 (2024), https://pubs.aip.org/aip/mre/article-pdf/doi/10.1063/5.0196125/19853669/037204_1_5.0196125.pdf.

[24] B. King and N. Elkina, "Vacuum birefringence in high-energy laser-electron collisions," Phys. Rev. A **94**, 062102 (2016).

[25] Yousef I. Salamin, Guido R. Mocken, and Christoph H. Keitel, "Electron scattering and acceleration by a tightly focused laser beam," Phys. Rev. ST Accel. Beams **5**, 101301 (2002).